JOURNAL OF MATERIALS SCIENCE 28 (1993) 729–734

Sintered iron-ceramic composites

S.K. MUKHERJEE, B. COTTERELL, Y. W. MAI
Department of Mechanical Engineering, The University of Sydney, New South Wales 2006, Australia

In order to improve the strength and high-temperature properties of sintered iron, iron–ceramic composites have been studied. In the present investigation, iron powder with 0–8 vol % Al_2O_3 or SiC particles of different sizes were selected for the study. Powders were mixed, compacted and subsequently sintered at 1150°C under an endo gas atmosphere. Various properties of the sintered compacts, such as density and mechanical properties, were evaluated. Fractography, microstructural studies including EDAX, X-Ray image analysis were studied for selected specimens. It was established from the results that 4 vol % Al_2O_3 or SiC are optimum to obtain superior properties of the composites.

1. Introduction

Sintered iron components are used for various commercial applications. However, inferior strength is a limitation of sintered straight iron powder metallurgy products in many applications. Therefore, it is very important to find some way to increase the strength of straight iron powder metallurgy products. There is some reported work [1–5] on phosphorus-containing iron, and the effects of MCM on the effect of sintered iron and iron–carbon premixes. However, most sinterings were carried out in the relatively higher temperature range of 1300°C with achievement of limited ductility. The purpose of the present investigation was to increase the strength of iron by incorporating ceramic particles and sintered materials at relatively lower temperature, than is generally used in industry.

2. Experimental procedure

The following raw materials were used for the present investigation.

Iron: High compressibility water-atomized irregular particle structure iron powder, WPL-200 (Hoganas) was used as base material. The characteristics of the powder are as follows: carbon content 0.02%; silicon 0.05%; manganese 0.2%; phosphorus 0.02%; sulphur 0.015%; hydrogen loss 0.2%; apparent density 2.6 Mg m^{-3}; flow rate < 35 s/50 g; compressibility 6.95 Mg m^{-3} at 600 MPa; particle size < 63 μm $= 45\%$, > 63 μm $= 40\%$.

Alumina particles: fine (average size 1 μm), and coarse (average size 40 μm).

Silicon carbides: fine (average size 0.5 μm), and coarse (average size 5 μm).

Mixing of iron powder and Al_2O_3 or SiC dispersoid (0–8 vol %) was performed in a mixer for 1 h. From these powder premixes, dog-bone type green compacts were prepared in an hydraulic press at 450 MPa compaction pressure.

All green compacts were sintered in an industrial mesh-belt type furnace at 1150°C for 45 min under an Endo gas atmosphere. The total duration of the heating cycle during sintering was 4 h.

Densities of green and sintered compacts were determined from dimensional measurements as well as by the water-displacement method after coating the samples with hair-lacquer solution.

Densification parameters of all the specimens were calculated using the formula

$$\Delta D = \frac{\text{Sintered density} - \text{Green density}}{\text{Theoretical density} - \text{Green density}}$$

Rockwell B hardness was measured for the sintered samples. The tensile testing of the specimens were carried out on an Instron machine using a chart speed of 10^{-2}m min^{-1}. Percentage elongation was determined on 25 mm gauge length. Microstructures were studied under optical as well as scanning electron microscopes. Fractography of the specimens was examined using SEM. EDAX and X-ray image analysis under SEM were conducted on some of the selected specimens.

3. Results

3.1. Iron–Al_2O_3 composites

3.1.1. Sintered density

Sintered densities of the composites decrease with increase in Al_2O_3 content (Fig. 1). This is also reflected in the sintered porosity plot (Fig. 2).

3.1.2. Densification parameter

Fig. 3 shows the behaviour of densification parameter of iron and its composites. The densification parameter decreases in the presence of Al_2O_3 particles. However, the densification parameter for Al_2O_3-containing composites remains constant up to 4 vol % Al_2O_3 dispersoid in both fine (f) as well as

0022–2461

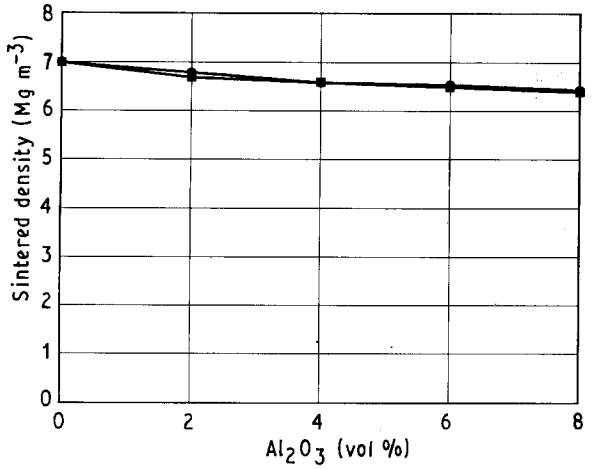

Figure 1 Sintered density of iron–Al_2O_3 composites. (●) Fine, (■) coarse.

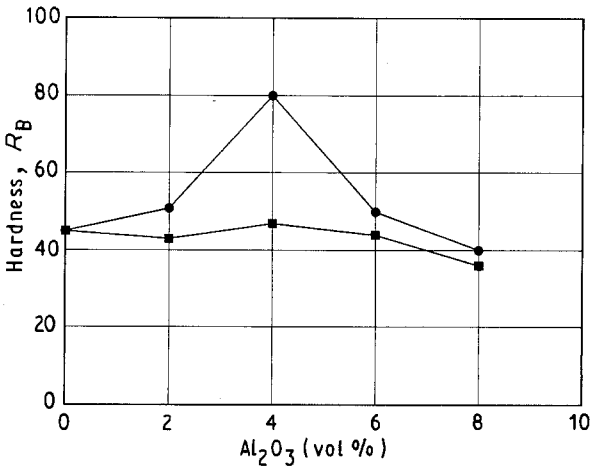

Figure 4 Hardness of sintered iron–Al_2O_3 composites. (●) Fine, (■) coarse.

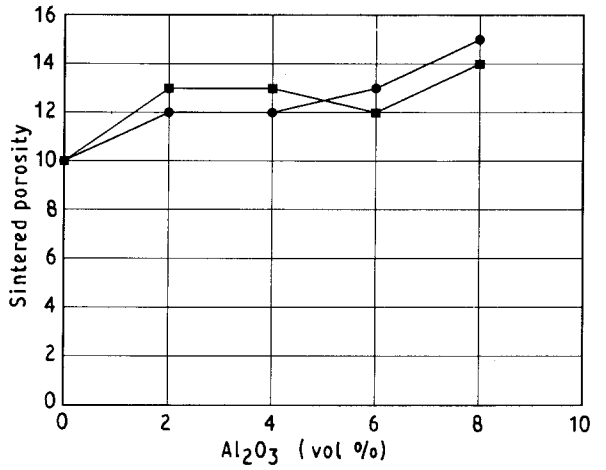

Figure 2 Sintered porosity of iron–Al_2O_3 composites. (●) Fine, (■) coarse.

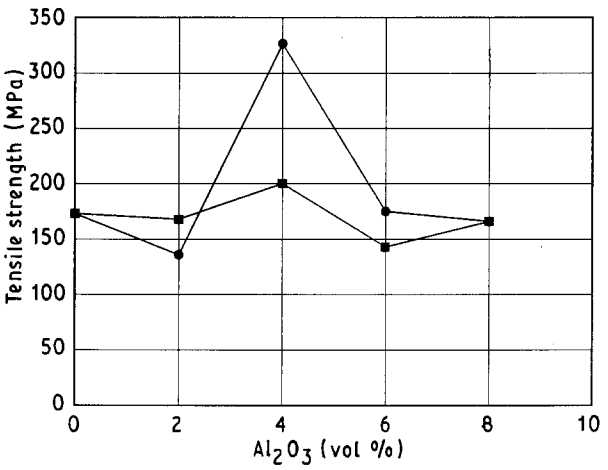

Figure 5 Tensile strength of sintered iron–Al_2O_3 composites. (●) Fine, (■) coarse.

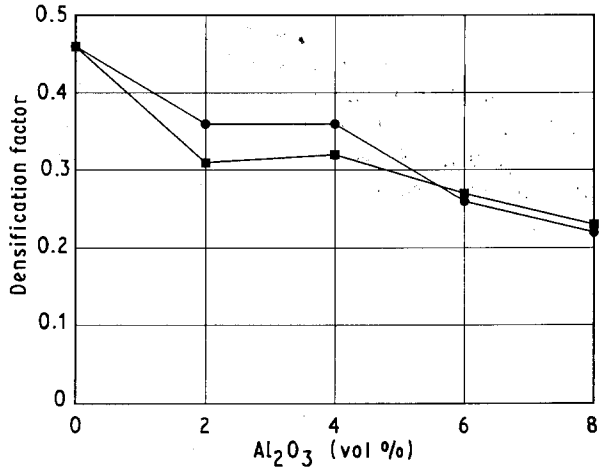

Figure 3 Densification parameter of iron–Al_2O_3 composites. (●) Fine, (■) coarse.

coarse (a) particles. It decreases steadily with further Al_2O_3 addition.

3.1.3. Hardness

It is interesting to note from Fig. 4, that a significant increase in hardness is achieved in the case of 4 vol % fine Al_2O_3-containing composite. In general, hardness is maximum for 4 vol % Al_2O_3-containing composites in both particle sizes.

3.1.4. Tensile strength

The effect of hardness is clearly reflected in tensile strength behaviour of the materials (Fig. 5). The tensile strength of 4 vol % Al_2O_3-containing composites are higher than any other compositions. There is a remarkable increase in tensile strength in the case of 4 vol % Al_2O_3 (fine particle size)-containing composite. It has been observed that straight iron compact exhibits a percentage elongation of 5% while other composites fail in a brittle manner. This feature is observed from fractographs. Fig. 5 shows some dimple-type fracture for straight iron as compared to intergranular composite fracture.

3.2. Iron–SiC composites

3.2.1 Sintered density

The behaviour of the sintered density of SiC-containing composites (Fig. 6) shows the similar behaviour of

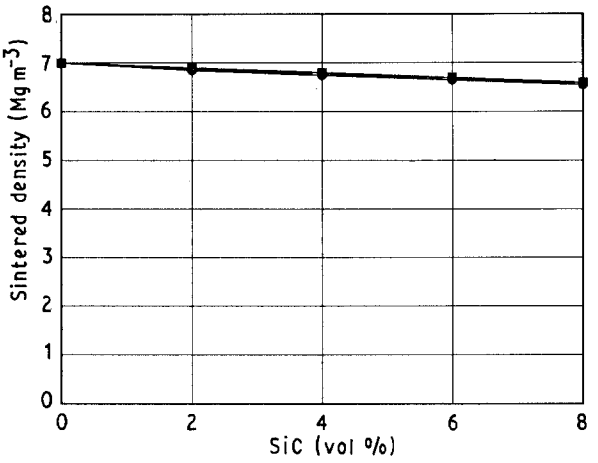

Figure 6 Sintered density of iron–SiC composites. (●) Fine, (■) coarse.

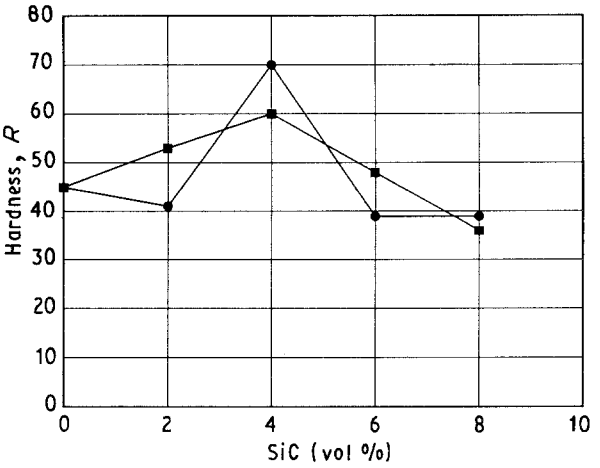

Figure 9 Hardness of sintered iron–SiC composites. (●) Fine, (■) coarse.

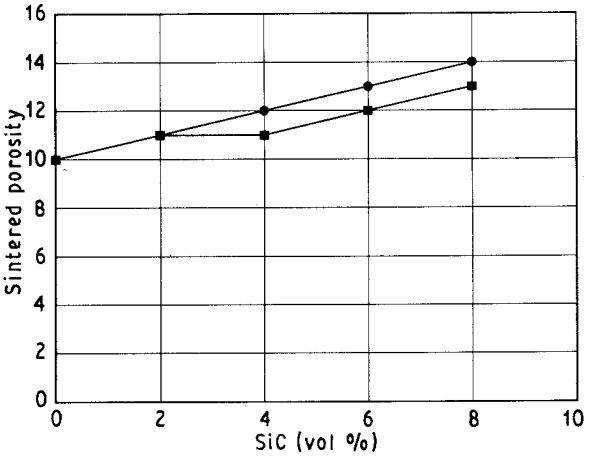

Figure 7 Sintered porosity of iron–SiC composites. (●) Fine, (■) coarse.

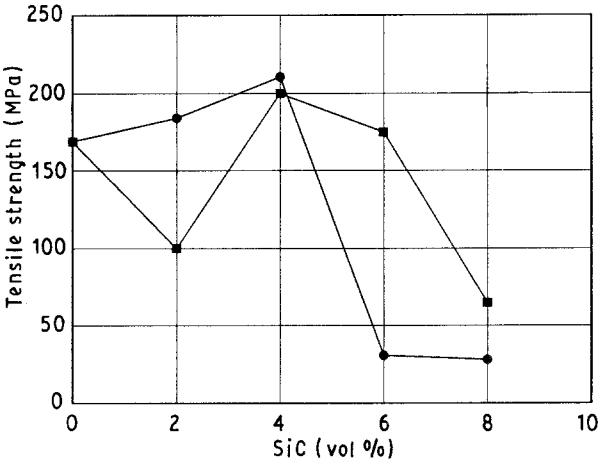

Figure 10 Tensile strength of sintered iron–SiC composites. (●) Fine, (■) coarse.

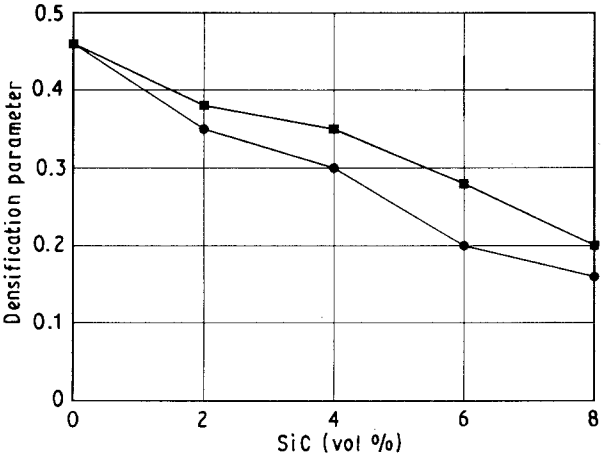

Figure 8 Densification parameter of iron–SiC composites. (●) Fine, (■) coarse.

Al_2O_3-containing composites. Sintered porosity (Fig. 7) also decreases with increase in SiC content in the composites.

3.2.2. Densification behaviour

Unlike Al_2O_3- containing composites there is no arrest (Fig. 8) in the densification parameter behaviour: it decreases steadily with increase in SiC dispersoid in the alloys.

3.2.3. Hardness

Hardness (Fig. 9) is maximum for 4 vol % SiC (fine particle size) - containing composites as in the case of Al_2O_3 - containing composites. In general, maximum hardness is obtained around 4 vol % SiC-containing composites.

3.2.4. Tensile strength

The tensile strength of the components shows (Fig. 10) that the presence of 4 vol % SiC increases the strength of iron in both particle sizes. However, the strength decreases drastically beyond 4 vol % SiC, particularly for fine SiC-containing composites. No elongation was observed for any of the SiC containing composites.

3.2.5. Microstructures and Fractography

Fig.11 shows the optical micrographs of sintered iron, its composites with 4 vol % Al_2O_3 or SiC. It appears

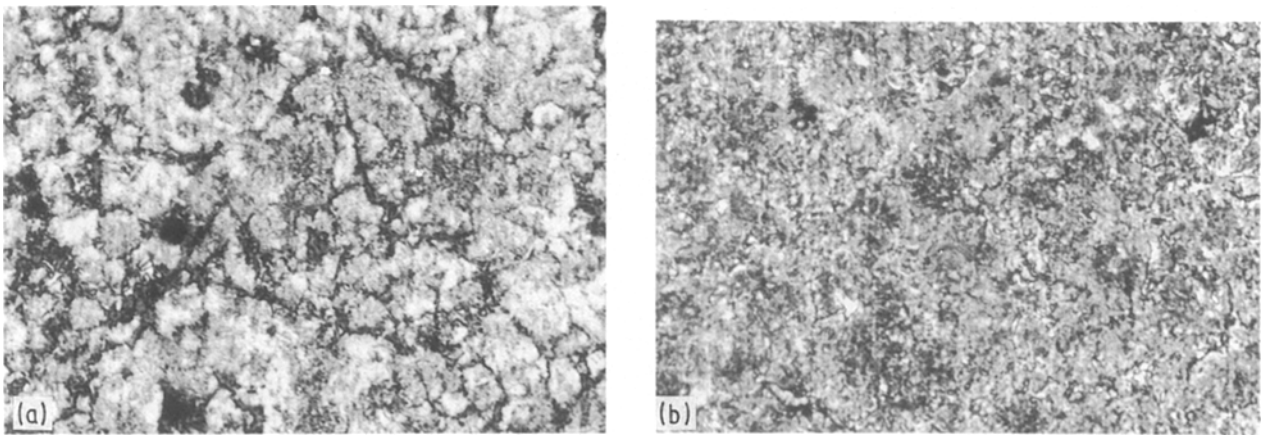

Figure 11 Optical micrographs of (a) sintered iron and (b) sintered iron + 4 vol % Al_2O_3 particles (f). × 100

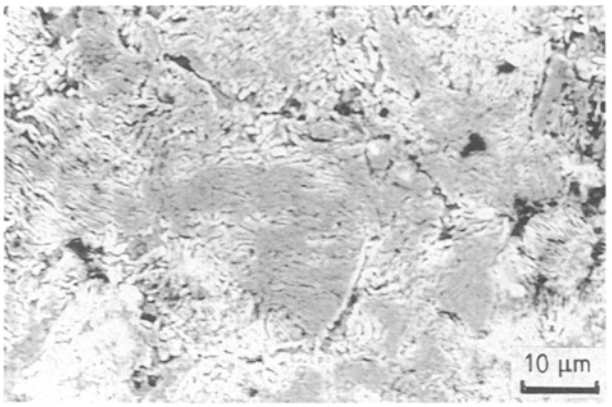

Figure 12 Scanning electron micrograph of sintered iron–ceramic (f) composites.

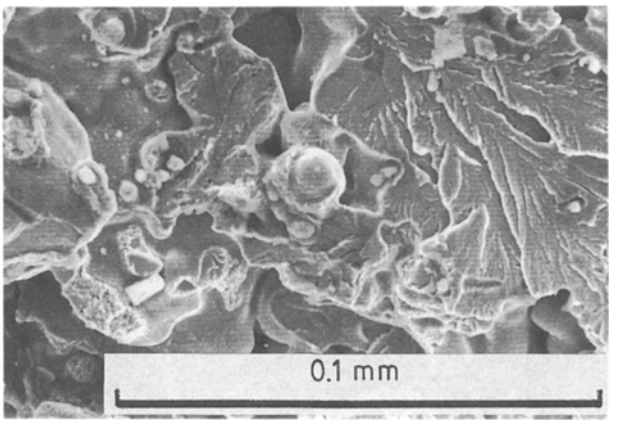

Figure 15 Fractograph of sintered iron–4 vol % Al_2O_3 (f) composite.

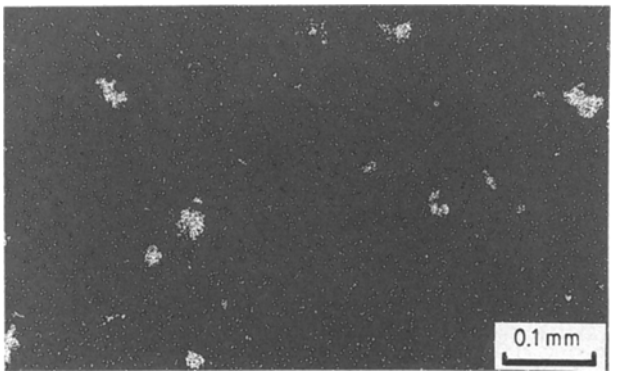

Figure 13 X-ray image analysis of sintered iron–4 vol % SiC (f) composites.

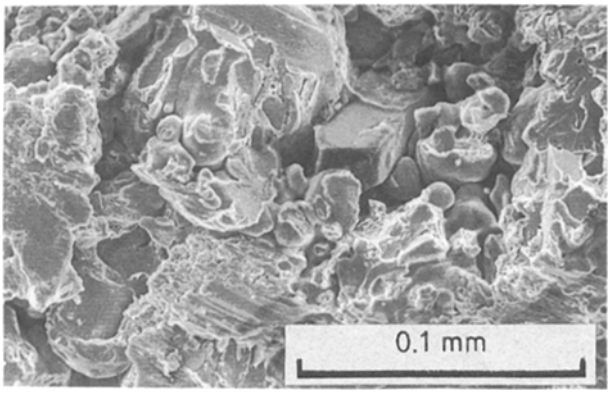

Figure 16 Fractograph of sintered iron–4 vol % SiC (f) composite.

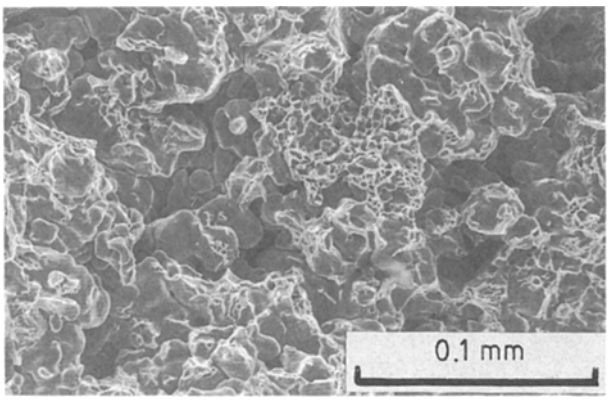

Figure 14 Fractograph of sintered iron.

from the micrographs there is little difference in the microstructure except the distribution of porosity and their sizes. Fig. 12 shows a scanning electron micrograph of the composites which indicates the distribution of the Al_2O_3 or SiC particles in the matrix. X-ray image analysis (Fig. 13) shows the more or less even distribution of dispersoids. Figs 14–16 show the fracture behaviour of iron and its composites. Straight iron shows some dimple-type fracture whereas it is cleavage type in the case of composites. EDAX (Figs 17 and 18) show the presence of Al_2O_3 and SiC

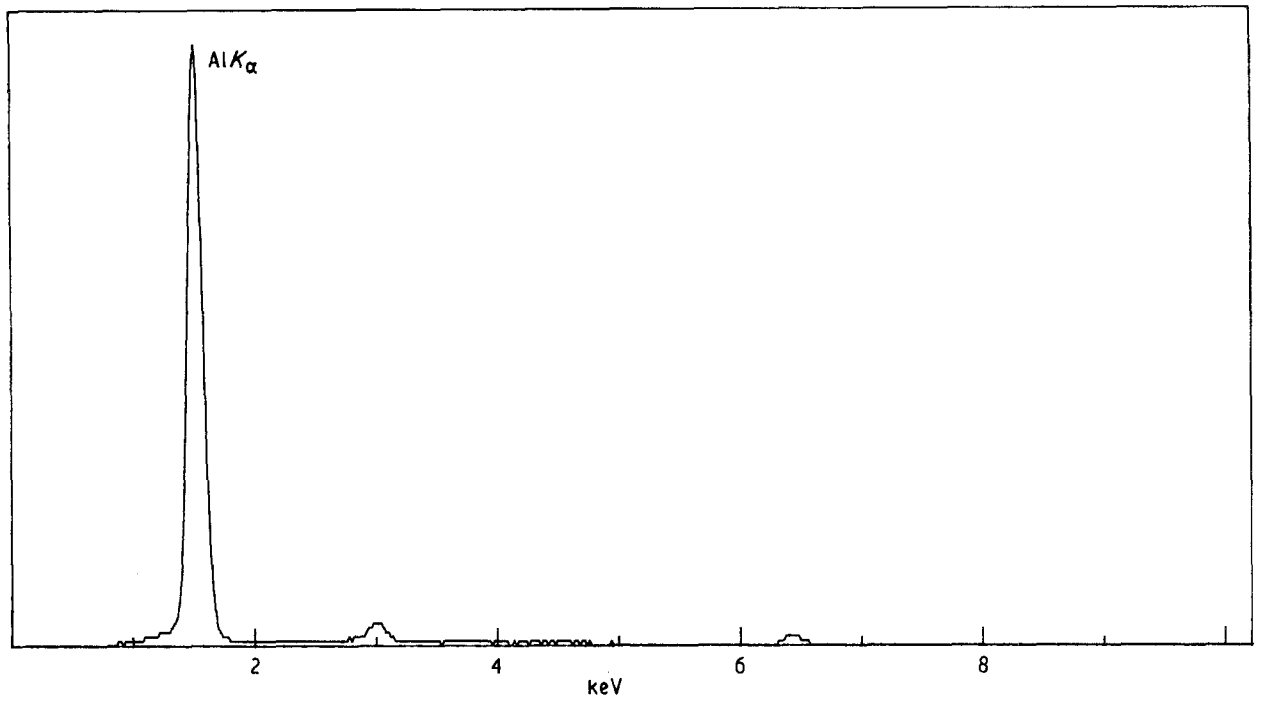

Figure 17 EDAX of fractured iron–4 vol % Al_2O_3 (f) composite.

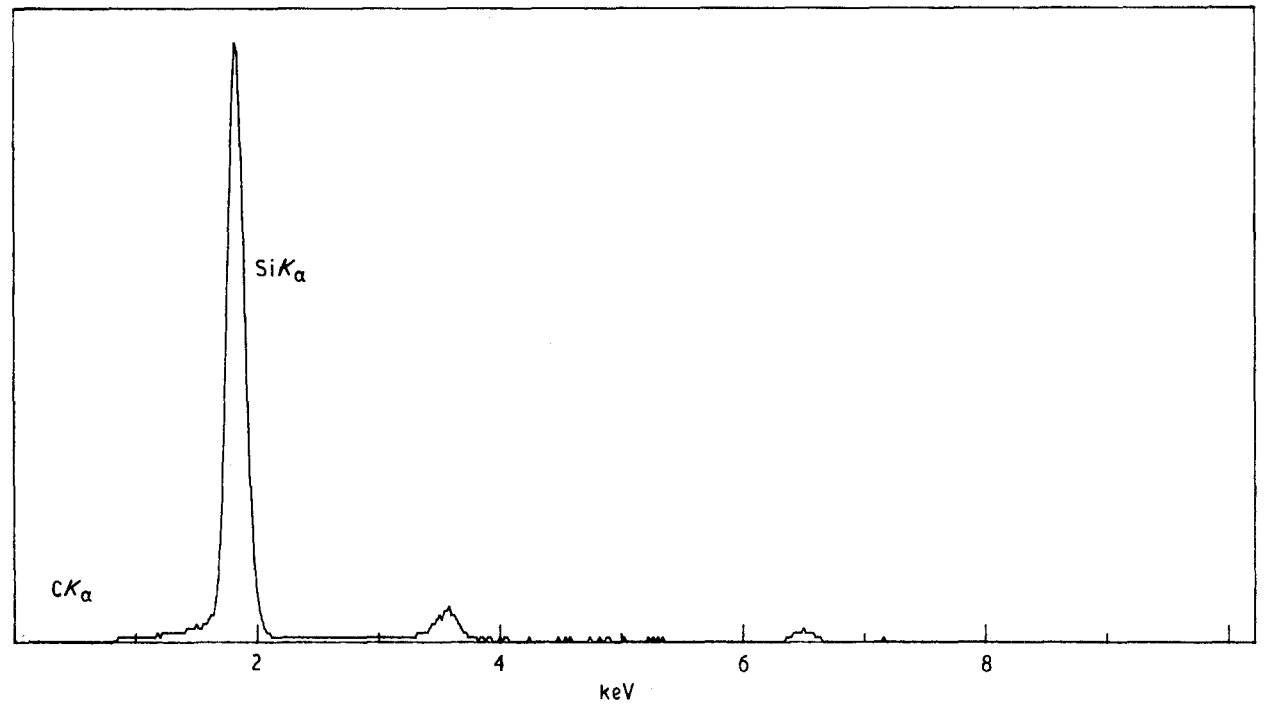

Figure 18 EDAX of fractured iron–4 vol % SiC (f) composite.

particles of the corresponding fractographs of Figs 15 and 16, respectively.

4. Discussion

4.1. Densification behaviour

The results (Figs 3 and 10) show that the densification is higher for straight iron compared to Al_2O_3- or SiC-containing composites, which is obvious. The presence of ceramic particles inhibits the sinterability of the composites as more metal–metal bonding is replaced by metal–ceramic or ceramic–ceramic bonds which have less diffusivity compared to straight iron.

4.2. Hardness

The hardness reaches a maximum for 4 vol % dispersoid containing composites either of Al_2O_3 or SiC for their fine particle sizes. This is due to dispersion hardening of the composites as particle sizes are below 1 μm in these cases. This is confirmed, because improvement of remarkable hardness is more or less

absent for coarse dispersoids like Al_2O_3 where particle size is over 40 μm. However, the beneficial effect of hardening for more than 4 vol % dispersoid-containing composites is not achieved, due to poor particle bonding in the composites. That observation is confirmed from low ΔD values of the respective alloys (Figs 3 and 10).

4.3. Tensile strength

The remarkable increase in strength of 4 vol % Al_2O_3 (fine particle size) -containing composite is the direct consequence of the dispersion-strengthening effect. It is confirmed from the investigation that 4 vol % Al_2O_3 is optimum for the present alloy system. It was found that the densification parameter values for 2 and 6 vol % Al_2O_3-containing composites are close to the D value of its 4 vol % composite, although their strength values are much lower than the 4 vol % composite. This can be explained by the Orowan mechanism of strengthening. The effect of strengthening is not achieved as the particle distance is too far for 2 vol % Al_2O_3 and too close for 8 vol % Al_2O_3 dispersoids to impart a significant beneficial effect in the alloy.

Similar behaviour is also observed in case of SiC-containing composites, as maximum improvement in properties is achieved in the case of 4 vol % dispersoid.

It is noticed from the present study that the dispersion strengthening is more effective than particulate strengthening, because properties are well below those for coarse particle (40 μm Al_2O_3) dispersoid - containing composites, compared to the similar compositions with fine particles (< 1 μm).

4.4. Fractography

It is clear from fractographs (Figs 14–16) that the presence of an inert second phase increases the brittleness of the materials, because it exhibits cleavage fracture compared to straight iron (Fig. 14), which shows some dimple behaviour. Therefore, it is doubtful if this particulate composite can improve the room-temperature toughness of the material, although our work [6] indicated that toughness of the material will certainly be improved using Al_2O_3 fibre for a similar matrix.

5. Conclusions

The following conclusions can be drawn from the present investigation.

1. Sinterability of the straight iron is higher than its composites. The densification parameter steadily decreases with increase in dispersoid content.
2. 4 vol % dispersoid is optimum to impart better mechanical properties of the alloy.
3. 4 vol % Al_2O_3 (fine particle size)-containing composite is superior to any other composition.
4. Al_2O_3-containing composites are better than SiC containing composites.
5. Ductility was reduced to zero when any dispersoid was added to straight iron powder.
6. Straight iron shows some dimple-type fracture, whereas composites show cleavage-type fracture.

Acknowledgements

Financial support by ARC to this project is appreciated. The authors are grateful to ASTRA Engineering, Sydney for providing facilities to carry out some of the experiments.

References

1. H. J. RETELSDORF, R. M. FICHTE, G. HOFFMANN and K. DALAL, *Metal.* **29** (1975) 1002.
2. G. ZAPF and K. DALAL, "Modern Development in Powder Metallurgy", Vol. 10, edited by H. H. Hausner and P. W. Taubenblatt (MPIF, Princeton, NJ, 1975) p. 129.
3. G. ZAPF, G. HOFFMANN and K. DALAL, *Powder Metall,* **18** (1975) 214.
4. Md. HAMIUDDIN and G. S. UPADHYAYA, *Powder Met. Int.* **12** (2) (1980) 65.
5. V. B. PHADKE and B. L. DAVIES, *Int. J. Powder Met. Powder Tech.* **13** (1977) 25.
6. S. K. MUKHERJEE, B. COTTERELL and Y. W. MAI, in "Diffusion Defect Data, Part B, 1992, Sintering '91", p. 523–30.

Received 8 October 1991
and accepted 11 June 1992